



Odyssa – a techno-economic evaluation framework for wind-assisted vessels with hydrogenation

Annika Fitz, Dheeraj Gosala, Vaidehi Gosala, Tobias Lampe, Thorben Schwedt, Sophie Stutz & Sören Ehlers

To cite this article: Annika Fitz, Dheeraj Gosala, Vaidehi Gosala, Tobias Lampe, Thorben Schwedt, Sophie Stutz & Sören Ehlers (08 Aug 2025): Odyssa – a techno-economic evaluation framework for wind-assisted vessels with hydrogenation, Ships and Offshore Structures, DOI: [10.1080/17445302.2025.2529961](https://doi.org/10.1080/17445302.2025.2529961)

To link to this article: <https://doi.org/10.1080/17445302.2025.2529961>



© 2025 German Aerospace Center (DLR),
Institute of Maritime Energy Systems



Published online: 08 Aug 2025.



Submit your article to this journal [↗](#)



Article views: 77










View related articles [↗](#)



View Crossmark data [↗](#)

Odyssa – a techno-economic evaluation framework for wind-assisted vessels with hydrogeneration

Annika Fitz , Dheeraj Gosala , Vaidehi Gosala , Tobias Lampe , Thorben Schwedt , Sophie Stutz  and Sören Ehlers 

German Aerospace Center (DLR e.V.), Institute of Maritime Energy Systems, Geesthacht, Germany

ABSTRACT

In this paper the modelling framework Odyssa is presented, which combines several aspects such as the performance of vessel and wind-assisted propulsion devices, powertrain modelling, operation optimization and route simulation with time-resolved weather data to analyse ship design, as well as operational and economic aspects. The framework is illustrated by a case study on a sailing bulk carrier operating between Hamburg and New York. The model ship is equipped with a Dynarig sail system and an electrified powertrain with a methanol genset and a battery. Additionally, two hydrogenerators are available to recuperate energy during high wind conditions. The case study is performed for two operational speeds and the results are compared with two baseline designs: the first based on a classical two-stroke HFO engine and the second additionally equipped with sails. Results indicate that Dynarig sails can enable 36% fuel savings at a constant speed of 10 kn and 49.3% fuel savings when instantaneous vessel speed is optimized without compromising on the average speed. When the average speed is reduced to 7 kn, hydro-generators are found to be particularly effective, unlocking a further 3.1% fuel savings on top of the results with speed optimization. By reducing fuel costs and mitigating emission taxes the investigated wind ship designs without recuperation resulted in similar total costs of ownership compared to a conventional baseline ship, despite higher investment costs on the sails system. Adding a recuperation system resulted in moderately higher costs.

ARTICLE HISTORY

Received 15 January 2025
Accepted 1 July 2025

KEYWORDS

Wind-assisted propulsion; hydrogeneration; ship and energy system modelling; speed optimization; route simulation; techno-economic analysis

1. Introduction

Wind propulsion systems are adaptable to both new build and retrofit vessels and reduce energy consumption, emissions, and dependence on fossil or renewable fuels. Promoted by advancements in the technology, both the quantity (Allwright 2024) and scale of the installations are on the rise (NEOLINE 2023; Singleton 2023). The implementation of increasingly larger sails alters the requirements on the ship design and operation strategy being tailored specifically to wind propulsion. To achieve this, simulation and assessment tools are needed, which combine aspects of sailing yachts and large commercially operating ships. Novel wind-propelled ship concepts, being able to use sails as the main propulsors, may include high side force producing hull shapes and appendages to counterbalance the side force production of large sails and to fully exploit sailing capabilities (Dykstra Naval Architects 2013; Seguin et al. 2019). During operation, speed optimization and wind routing can become a pivotal factor in the overall energy

balance of the ship, while at the same time complying to schedules. The application of hydrogenerators may offer additional potential for harnessing wind energy for hoteling, self-sufficient operation and energy production. At the the same time effects on the cargo space and weight and costs may not be neglected. Assessment tools of windship designs therefore need to cover a complex combination of various aspects.

In order to determine the energy consumption and recuperation potential it is key to accurately capture the interaction between the wind-powered propulsor (e.g. sail, Flettner rotor), the ship hull, the propeller and, if applicable, a hydrogenerator. Various works on ships with wind-assisted propulsion addressed this by quantifying each of the acting forces in multiple degrees of freedom and determining an equilibrium in various operating conditions (Tillig et al. 2017; Tillig and Ringsberg 2019; van der Kolk et al. 2019; Reche-Vilanova et al. 2021; Kramer and Steen 2022). This methodology

CONTACT Annika Fitz  annika.fitz@dlr.de  Institute of Maritime Energy Systems, German Aerospace Center (DLR e.V.), Geesthacht, 21502, Germany

© 2025 German Aerospace Center (DLR), Institute of Maritime Energy Systems

This is an Open Access article distributed under the terms of the Creative Commons Attribution License (<http://creativecommons.org/licenses/by/4.0/>), which permits unrestricted use, distribution, and reproduction in any medium, provided the original work is properly cited. The terms on which this article has been published allow the posting of the Accepted Manuscript in a repository by the author(s) or with their consent.

is known from sailing yacht design as ‘Velocity prediction program’ (VPP). The quantification is often based on empirical formulas to achieve sufficient accuracy as well as fast computational speed. In some cases, results of computational fluid dynamics (CFD) and model tests may be incorporated or used as a validation basis.

A hydrogenerator may be implemented into the VPP either as a propeller used in reverse (dual-use) unit (Liu et al. 2018) or as a dedicated hydrogenerator, solely used for recuperation (Ekinici and Alvar 2017). For the latter, resistance may be reduced out of operation, for example by folding the blades (Ekinici and Alvar 2017) or retraction from the water (watt&sea 2025). Previous works have proposed ship concepts with hydrogenerators for energy efficiency and self-sufficient operation (Alfonsin et al. 2015; Juliá et al. 2020; van der Plas et al. 2024) and energy harvesting (Babarit et al. 2020; Ouchi et al. 2023). The evaluation of the energy gain in relevant operating conditions was estimated based on the general performance characteristics of the ship concept (Babarit et al. 2020; Ouchi et al. 2023), a limited number of sample routes (Alfonsin et al. 2015) or probabilistic weather distributions (Juliá et al. 2020; van der Plas et al. 2024). To our knowledge no evaluations on energy gains with numerous full voyage simulations and developing weather conditions have been performed.

To model the efficiency losses of energy storage and consumption, the analyzed literature on windships utilized steady state models of the ship energy system components, representing the individual efficiency and limitations of each component at various operating points. This includes the specific fuel oil consumption (SFOC) curves of diesel engines (Tillig et al. 2017; van der Kolk et al. 2019), efficiency and state-of-charge of battery systems (Thies and Ringsberg 2022), and conversion rates and auxiliaries of P2X-systems (Alfonsin et al. 2015; Babarit et al. 2020). In previous works, only fully battery-electric systems or P2X systems were considered in combination with hydrogenerators. We propose using hydrogenerators in conjunction with hybridized systems of combustion engines and batteries, aiming at both (i) High operating range at high energy density through diesel or methanol combustion and (ii) the possibility of renewable energy harvesting and storage in a battery system, thereby reducing the amount of additional fuelling. We present such a concept in the case study in Section 3.

The speed and route of windships can be optimized to further improve their performance. Wind propelled vessels are particularly sensitive to their encountered operating conditions, which can be influenced by the ship speed, the flexibility of departure and arrival time, as well as the ship route (van der Kolk et al.

2019; Sun et al. 2022; Thies and Ringsberg 2022; Mason et al. 2023).

Studies on windship concepts often applied economical metrics to evaluate not only technical but also economic feasibility. Talluri et al. (2016) conducted a techno-economic study on vertical axis wind turbines for a Ro-Ro steel transporter using gas turbines or diesel engines. Using the TERA framework, they assessed economic feasibility through net present value, discounted payback period, and internal rate of return, identifying financial conditions for a target payback period. However, they did not account for system weight/volume or carbon tax. Later, the same group analyzed Flettner rotors on the same ship across four routes, incorporating carbon taxes (Talluri et al. 2018). The transport economics model of the ShipCLEAN (Tillig and Ringsberg 2020) framework further considered daily income as a function of the load factor, cargo capacity and freight rate, and applies it to speed optimization and wind assisted propulsion. The daily profit was then calculated by accounting for the income, operational costs and journey time, which could be used for further operational optimization. While installation costs were considered, carbon taxes or other environmental levies were not considered. Studies for non-wind propelled ships in literature have compared the economic benefits of using different advanced fuels and energy systems applying metrics such as total cost of ownership (covering capital costs, fuel costs, cost of storage and reduced cargo) (Horvath et al. 2018; Korberg et al. 2021) and levelized cost of mobility (LCOM). To the best of the authors’ knowledge, powertrain design exploration considering a total cost of ownership analysis, while considering weight and volume has not been performed before for powertrains with sails.

Through full voyage simulations under developing weather conditions, speed optimization and the integration of a hydrogenerator setup, we provide novel insights into the holistic performance evaluation and potential of wind-propelled ships with recuperation. In our economic evaluation, we incorporate key overlooked aspects, such as the inclusion of carbon tax considerations and the impact of added weight and cargo capacity loss. Additionally, we conduct a powertrain design exploration to optimize the balance between the wind propulsor and the powertrain system. The paper is structured as follows: Section 2 provides a general description of the utilized framework and its modules, namely the vessel performance module, route simulation module, energy system module and techno-economic module. In Section 3, the framework is demonstrated through a case study of a vessel on a trans-Atlantic sailing route. The vessel includes four Dynarig sails, dedicated

hydrogenerator units and a hybrid energy system including a methanol engine and a battery. The case study specific assumptions used in the submodules of the Odyssa Framework to address this particular application case are described in detail. The results on energy efficiency and economic performance are presented. The overall performance of the model and its development potential are summarized in Section 4.

2. Odyssa framework

The Odyssa Framework builds up on state-of the art methods to holistically capture the technical and economic aspects of windship operation, with a specific emphasis on the exploration of range extending, energy self-sufficient and energy harvester ships.

Figure 1 illustrates the basic structure of the Odyssa simulation Framework, which employs a modular approach to enable handling of various application scenarios and research questions. Each module can be easily exchanged, enhanced, or adjusted based on the desired goal. For example, the techno-economic model could either entail sophisticated approaches involving time-projected costs for fuel and components of the complete system, or involve only operating costs for fuel usage at the current point in time.

The ship configurator allows to select and specify all relevant components of the hydro- and aerodynamic system ‘ship,’ such as the hull, sail, propeller and hydro-generator. In the configurator, either predefined components can be chosen, or custom components can be defined. This includes basic parameters, such as e.g. ship length and propeller diameter, but also technical information required for the performance calculation, such as characteristic curves of e.g. propeller thrust and hull resistance. While various configurations are available as a preset, new components can be easily integrated. The gathered information is then made available for the other sub-modules of the framework.

In the vessel performance module, a 4-DOF equilibrium state model is employed to determine the operation state of the vessel. Neglecting dynamic effects, balance equations for surge, sway, roll and yaw are set up and solved on the basis of the ship specification and the environmental parameters.

$$\sum X_i(T, \beta, \delta) = 0 \quad (1a)$$

$$\sum Y_i(T, \beta, \delta) = 0 \quad (1b)$$

$$\sum N_i(T, \beta, \delta) = 0 \quad (1c)$$

$$\sum K_i(T, \beta, \delta, \Phi) = 0 \quad (1d)$$

Herein, X , Y , N , K indicate forces in surge direction, forces in sway direction, yaw moments and roll moments, respectively. The index i denotes the respective contributors to each balance, e.g. calm water resistance and wave resistance for Equation (1a).

After the equation system had been set up, it is solved for the variables thrust (T), drift angle (β), rudder angle (δ) and roll angle (Φ). In order to set up Equations (1a)–(1d), the complete system specification, including the sail trim angle, needs to be given. At this point, however, it is not known which sail trim angle is associated with the optimal vessel state, therefore requiring an optimization procedure. The optimization was realized as a simple sweep across all feasible trim angles. If there was no solution to the equation system (e.g. because hull, rudder and appendages could not produce enough side forces to counteract the sails), or if the vessel maximum roll angle was exceeded, the power for the respective trim angle is set to positive infinity. Otherwise, the required additional thrust (propeller usage) or the permissible additional resistance (negative thrust, turbine usage) is passed to the module responsible for the propulsion & recuperation unit.

Approaches of varying complexity can be employed to assess the propulsor and recuperation devices. Models for fixed pitch propellers, controllable pitch propellers, POD systems and turbines are currently available. In this work, the operation state of the propeller and the recuperation turbine is obtained by means of characteristic curves. Both units are treated mathematically the same. The propeller efficiency is labelled η_{prop} . The power coefficient C_P indicates how well a turbine can convert the energy contained in an incident flow into electrical energy. It is commonly used to evaluate the efficiency of standing turbines operating in wind or tidal flows. η_{Turb} relates the braking power of the towed turbine, which slows down the ship and is considered a cost of operating the turbine, to the electrical power the turbine can gain. The hydrodynamic characteristic curves are calculated using the following equations:

$$J = \frac{v}{nD} \quad k_T = \frac{T}{\rho n^2 D^4} \quad k_Q = \frac{Q}{\rho n^2 D^5} \quad (2a)$$

$$C_D = \frac{8F}{\pi \rho v_A^2 D^2} \quad C_P = \frac{2\pi n Q}{0.5 \rho v_A^3 \pi R^2} \quad (2b)$$

$$\eta_{prop} = \frac{J k_T}{2\pi k_Q} = \frac{T v_A}{2\pi n Q} \quad \eta_{Turb} = \frac{C_P}{C_D} = \frac{2\pi n Q}{F v_A} \quad (2c)$$

The advance coefficient J represents the speed ratio between inflow velocity and rotational speed of propeller or turbine. T stands for the thrust, Q for the torque, F

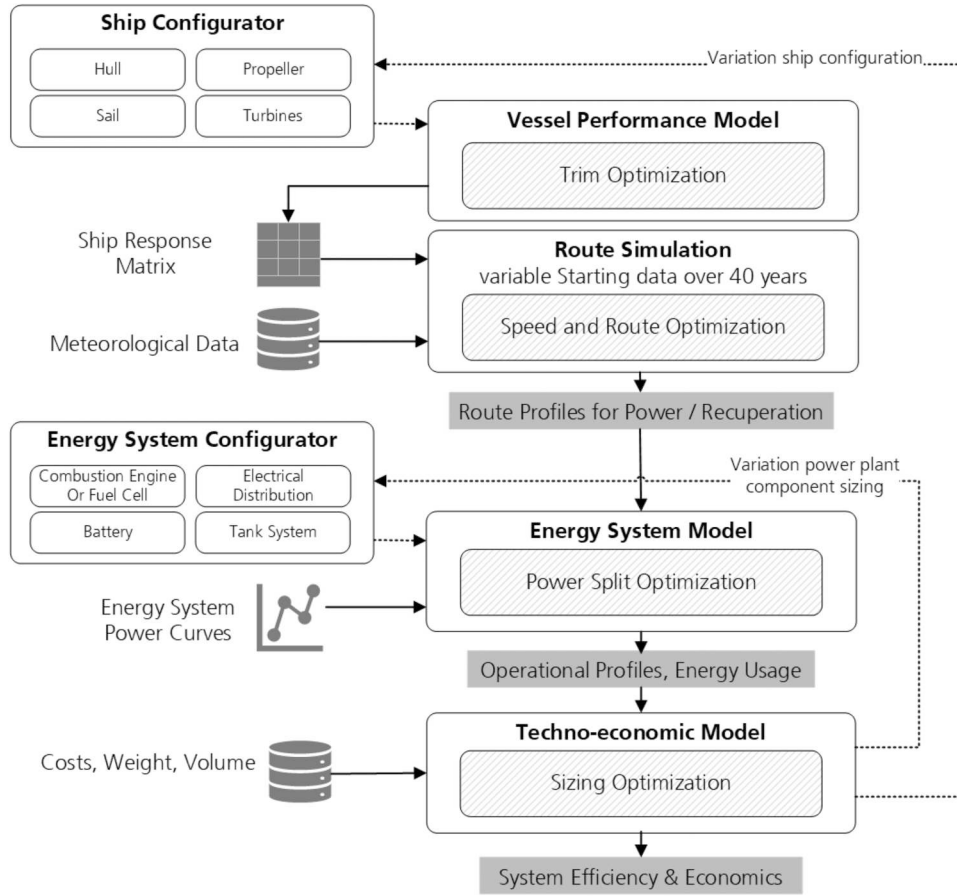


Figure 1. Schematic of the simulation framework. (This figure is available in colour online.)

for the drag force (negative thrust) of the turbine, n for the rotational speed, ρ for the water density, v_A for the inflow velocity to propeller or turbine and D for the diameter of its blades. Since the inflow to the turbine effects the power coefficient C_P , the recuperable power of the turbine increases with increasing ship speed. The characteristic curves of propeller and turbine are modelled as third-order polynomials. Given required / available thrust and ship speed the equations are solved for their zero points which deliver the necessary rotational speed. The roots of the third-order polynomials of the form

$$y^3 + 3py + 2q = 0 \quad (3)$$

are determined using the analytical Cardan equation according to Bronstein and Semendjajew (1977).

$$u_{1,2} = \sqrt{[3]-q \pm \sqrt{q^2 + p^3}} \quad (4)$$

$$y_1 = u_1 + u_2 \quad (5)$$

Based on the speed of the propeller or turbines, the torque is calculated directly from the characteristic curves. The results are checked for feasibility by comparing

them with the torque limitation curve of the propulsion motor or generator.

While it would be possible to integrate the vessel performance module directly into subsequent modules, usage of a *Ship Response Matrix* (SRM) as an intermediary is favourable with regard to calculational effort and re-usage of calculation results in multiple simulations. For all possible combinations of a given range of environmental parameters and ship speeds, the system operation state is calculated and the results are saved in the SRM. Provided the range of the respective parameters is resolved with suitable accuracy, results for arbitrary parameter values within the given range can then be obtained by means of interpolation.

Utilizing the SRM, route simulation can be performed. In this case, multiple techniques are available in *Odyssa's* routing module, ranging from fixed routes and velocities to speed optimization along a fixed route and, finally, route optimization in which only start and end events are fixed. Here, speed optimization along a fixed route is employed.

The overall route was divided into N sections, each of which were defined by the longitude and latitude coordinates (X_k, Y_k) and (X_{k+1}, Y_{k+1}) . The

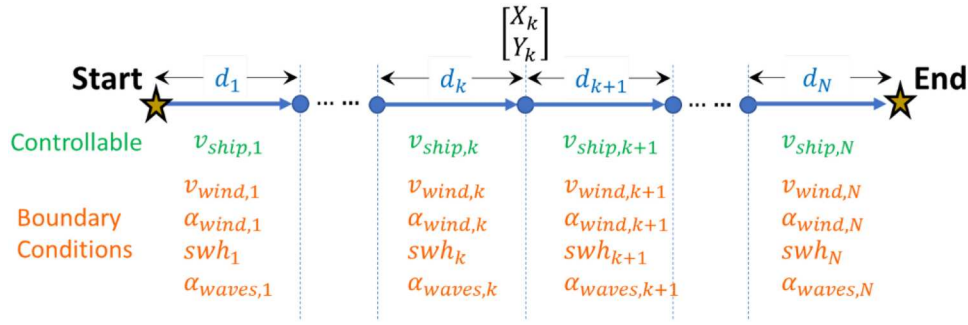


Figure 2. Speed optimization aims to find the optimal sequence of ship speeds for the journey from the beginning (X_0, Y_0) to the end (X_N, Y_N), based on time and location-dependent weather conditions. (This figure is available in colour online.)

ship traversed each section at a constant speed of $v_{ship}[k]$. The ship encountered different environmental conditions (wind velocity $v_{wind}[k]$, wind angle $\alpha_{wind}[k]$, sea wave height $sw_h[k]$, wave angle $\alpha_{waves}[k]$) at each section, depending on the time it was present in that location. The speed optimization problem aims at determining the optimal sequence of ship speeds ($v_{ship}[1], v_{ship}[2], \dots, v_{ship}[N]$) between the start and the end along the route (X_i, Y_i), as illustrated by Figure 2

The cost function may be adapted individually to the ship design optimizing for minimal energy use or energy harvest while complying with the use-case specific operation and time constraints. The optimization problem is solved using dynamic programming (DP), which can find the globally optimal solution for any nonlinear problem. The method requires that the weather along the route is known with certainty at different times. Therefore, while DP can be applied to analyse past routes where weather conditions are known, implementing this algorithm in real time requires other approaches. Notwithstanding the choice of optimization technique, route simulation is performed for a selected number of journeys. To this end, historical weather data of up to 40 years in the past, with time resolved wind and wave data, is made available. Due to the large time span of available data and the efficiency of the calculation method, it is possible to assess a large number of voyage simulations, which enables derivation of statistically relevant results with respect to investigated operational parameters and corresponding route profiles. At this point, the behaviour of the vessel with respect to aero- and hydrodynamic considerations is known, culminating in the required power demand to maintain propeller operation.

To holistically assess the ship system, enabling sophisticated investigations regarding energy storage and provision, the on-board energy system needs to be taken into account. The vessel energy system model receives the operating profiles of the ship as input data, which includes the propulsion power of the

propeller, the recuperation power of the hydrogenerators and the ship's auxiliary loads. Additionally, the specification of the energy system, as well as required system curves, need to be provided via the ship energy system configurator. In style of the configurator for the vessel, predefined as well as custom components can be used to specify the respective components, such as batteries and tanks, as well as the associated behaviour, e.g. (battery) loading curves and motor characteristics. To ensure that the load points are in compliance with the operating limits of the utilized machines in terms of speed and torque, corresponding limiting curve are integrated in the vessel performance model also. For hybrid systems, e.g. Diesel-battery or fuel cell- battery electric, an optimum power split algorithm can be applied. Simulations are conducted for the chosen set of ship energy system components, yielding an assessment of, for instance, the overall efficiency, fuel consumption including propulsion and hotel loads, on-board energy flows as well as associated operational profiles.

As a last step, the energy system sizing and costs are evaluated in the techno-economic model and compared to conventional baseline designs. Implementing new components into the ship energy systems, such as hydrogenerators and battery systems, increases the complexity of the system and requires a careful sizing synthesis to enable an energy-efficient interplay. At the same time the effects on overall costs must not be neglected. For example, for a small battery and hydrogenerator the power and energy recuperation is limited, while for a bigger one the system cost and weight are higher. This trade-off between the size and system cost and weight needs to be evaluated. For this, the cost effectiveness of the overall energy system needs to be analyzed to enable the determination of an energy system with minimum additional costs, and to compare to existing systems to understand overall feasibility. Making use of the power profiles derived in the route simulation and in turn the operational profiles provided by

the energy system model, as well as additional information on (projected) costs, weight and volume of fuel and (new) components, the economic performance of the system is assessed. Total cost of ownership (TCO), defined in (6b) is used as the primary metric for cost comparison, when the average speed of the baseline and the model ship with hydrogenerators is the same:

$$\begin{aligned} TCO = & \text{InitialCost} + \text{MaintCost} + \text{FuelCost} \\ & + \text{ReplCost} + \text{CO}_2\text{Cost} + \text{OpportunityCost} \end{aligned} \quad (6a)$$

$$\begin{aligned} \text{OpportunityCost} = & \text{UnitFreightCostOfCargo} * \\ & (\text{CargoCap}_{\text{baseline}} * \text{AnnMiles}_{\text{baseline}} \\ & - \text{CargoCap}_{\text{WAPS}} * \text{AnnMiles}_{\text{WAPS}}) \end{aligned} \quad (6b)$$

Here, the initial cost is the incremental capital cost of the system as compared to a baseline conventional ship, where the cost of unchanged components (such as propeller) are not considered; maintenance cost is calculated for the engines; replacement costs are calculated for the short life components such as battery and sails; the carbon emissions cost is calculated for the carbon emitted by the vessel only, the carbon emissions upstream are not considered here; and the opportunity cost is the amount of revenue lost due to reduced cargo carrying capability and reduced annual mileage in case of speed reduction. Additionally, the net present value, and the annualized cost per mile were considered to account for the time discounted value of money, as shown in (7a) and (8):

$$NPV = \text{InitialCost} + \sum_{i=1}^n \frac{TC}{(1+r)^i} \quad (7a)$$

$$\begin{aligned} TC = & \text{MaintCost} + \text{FuelCost} + \text{ReplCost} \\ & + \text{CO}_2\text{Cost} + \text{OpportunityCost} \end{aligned} \quad (7b)$$

$$\text{AnnCost} = \left(\frac{r \times NPV}{1 - (1+r)^{-n}} \right) / \text{AnnMiles} \quad (8)$$

where, n is the ship life (years), TC is the annual flow, r is the discount rate, and AnnMiles is the annual miles travelled. The annualized cost per mile gives a single number for comparing the considered technologies and the powertrain sizes.

To identify the most favourable energy system synthesis to attend to the energy needs as well as provide the lowest the TCO, the component sizes are varied according to a brute force DOE repeating the energy system simulations. The full workflow is conducted for the targeted ship design as well as a

conventional baseline case, which allows to compare the effects in system efficiency and economic performance.

With the described work flow, an in-depth assessment of a single configuration of vessel and energy system is possible. To find the most suitable specification for each system, two optimization loops are available, which allow for variation of the ship as well as energy system configuration. Sizing ranges can be applied to identify the optimum solution in terms of energy harvest and costs.

3. Case study

We utilized the Odyssa Framework to simulate a model ship of a sailing bulk carrier, see Figure 3, operating on an Atlantic route between Hamburg and New York.

The model ship was propelled by four large Dynarig sails, aiming to maximize the sail area and constitute the main propulsion system of the ship. To balance the high side forces of the wind propellers, the ship was equipped with a centreboard. In low wind conditions auxiliary propulsion power was delivered by an electrified powertrain, consisting of a electric motor powered by a methanol genset and a lithium-ion battery. On favourable conditions on the other hand two hydrogenerator units were submerged into the water to harvest renewable energy. To understand the benefits of implementing these technologies we compared the model ship with two alternative powertrain options: First, a conventional baseline ship without sails, operating on a two-stroke heavy fuel oil (HFO) engine with a purely mechanical powertrain. Second, an intermediate baseline ship, as well operating on sails and an electrified powertrain but without a hydrogenerator or a battery for energy storage. This choice was motivated by the intention to highlight the differences between a conventional ship to a ship utilizing wind-assisted propulsion, as well as a future-oriented motor concept, and in turn a ship utilizing wind-assisted propulsion, the novel motor concept, and energy recuperation. The main dimensions of the model vessel, kept constant for all powertrain options, are shown in Table 1. For the conventional baseline case, the sails, hydrogenerator and centreboard were not utilized.

Table 2 presents an overview on the analyzed powertrain options.

In the remainder of this section, the adaption of the Odyssa framework to the described case study is detailed and corresponding results are presented and discussed.

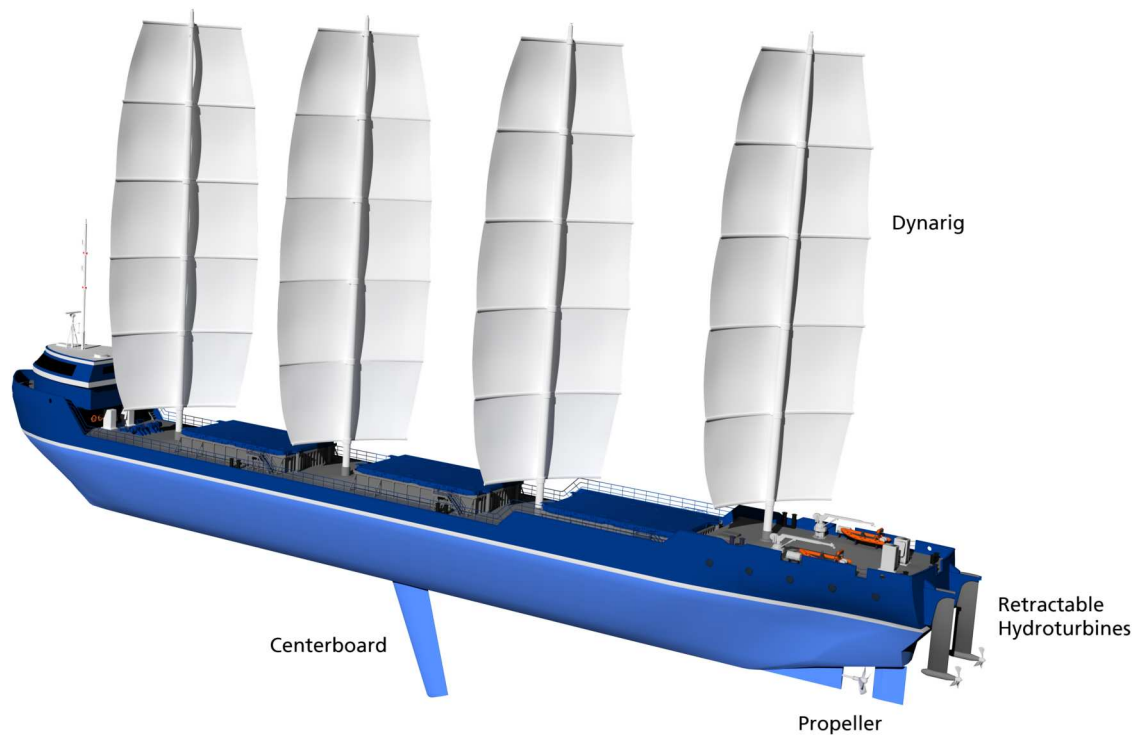


Figure 3. Model vessel. (This figure is available in colour online.)

3.1. Vessel performance model

The general form of the balance equations given in Equations (1a)–(1d) is applied to the described case study yielding the following balance equations:

$$X = 0 = X_{CW} + X_{AW} + X_D(\beta) + X_W + X_S + X_R(\delta, T) - T \quad (9a)$$

$$Y = 0 = Y_D(\beta) + Y_W + Y_S + Y_R(\delta, T) + Y_{CB}(\beta) \quad (9b)$$

$$N = 0 = N_D(\beta) + N_W + N_S + N_R(\delta, T) + N_{CB}(\beta) \quad (9c)$$

$$K = 0 = K_D(\beta) + K_W + K_S + K_R(\delta, T) + K_{CB}(\beta) - GM\Delta \sin(\Phi)g \quad (9d)$$

Table 1. Main dimensions of the model ship.

Characteristic	Value
Lenght over all	130 m
Breath	18.86 m
Draught (centreboard retracted)	7.9 m
Draught (centreboard extended)	20.3 m
Tonnage	12600 t
Sail Area	4000 m ²
Design speed	10 kn
Propeller Type	Fixed-pitch
Turbine Diameter	2 × 4 m

Individual contributions and the used indices are summarized in Table 3.

For calm water resistance, the Holtrop & Mennen model (Holtrop and Mennen 1982) was employed, while added resistance in wave was addressed by a method from Townsin and Kwon as reported in Molland et al. (2011). Forces and moments due to vessel drift were calculated based on considerations from Tillig and Ringsberg (2019). The influence of wind was captured using the Blendermann (1994) approach while the sails were considered by means of lift and drag coefficients of experimental data presented by Bordogna et al. (2018). Assuming standard profile geometries, rudder and centreboard were modelled via equations given by Bertram (2011).

For the fixed-pitch propellers, the classic Wageningen-B Series propeller curves was used with the

Table 2. Analyzed powertrain options.

Component	Baseline	Intermediate Baseline	Model Ship
Sails	–	Dynarig	Dynarig
Modes	Propulsion	Propulsion	Propulsion/Recuperation
Powertrain Type	ICE-mechanic	ICE-hybrid	ICE-hybrid
Engine Type	2-stroke HFO	2-stroke HFO /Methanol	2-stroke Methanol
Battery System	–	–	Li-Ion

Table 3. Summary of contributions to balance equations.

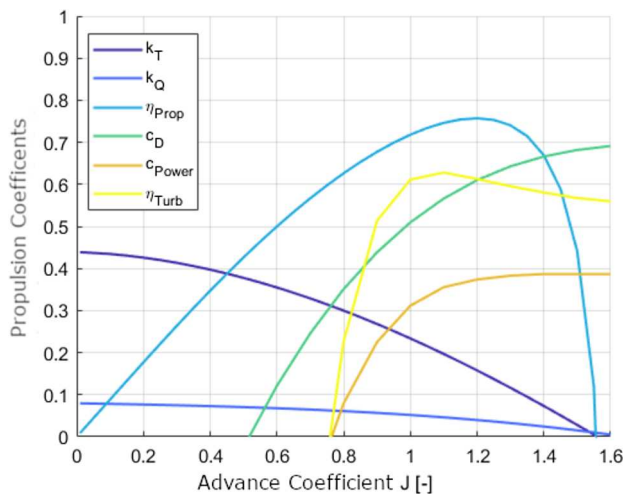
Variables	Description
X_{CW}	Calm water resistance
X_{AW}	Added resistance in waves
X_D, Y_D, N_D, K_D	Drift induced forces and moments
X_W, Y_W, N_W, K_W	Wind induced forces and moments
X_S, Y_S, N_S, K_S	Sail forces and moments
X_R, Y_R, N_R, K_R	Rudder forces and moments
$X_{CB}, Y_{CB}, N_{CB}, K_{CB}$	Center-board forces and moments

dimensionless thrust coefficient $k_T(J)$ and the dimensionless torque coefficient $k_Q(J)$, both as a function of the advance number J as given in Barnitsas (1981). The drag coefficient and power coefficient curves from Juliá et al. (2020) were re-used for the turbines. To retain comparability with the propeller, they are plotted against the advance coefficient (J) instead of the commonly used tip speed ratio (TSR). The hydrodynamic characteristics of the propeller and turbine are shown in Figure 4.

The turbine starts to turn at idle speed in the flow at $J = 0.5$, only generating resistance. From $J \sim 0.76$ onwards C_p assumes values > 0 and the turbine recuperates energy. If the propeller or turbine speed falls below 10 rpm, the model used only the sails for propulsion.

Having defined the setup of the performance model, the Ship Response Matrix of the investigated vessel was calculated. An excerpt of the results is given in Figure 5, which illustrates the interplay of sails, propeller and hydrogenerator. The presented results were obtained for zero wave height and an inflow angle between wind and ship forward direction of 105° .

The values are shown over ship speed at various wind speeds using the optimal sail trim. Positive power means mechanical propulsion power on the propeller shaft,

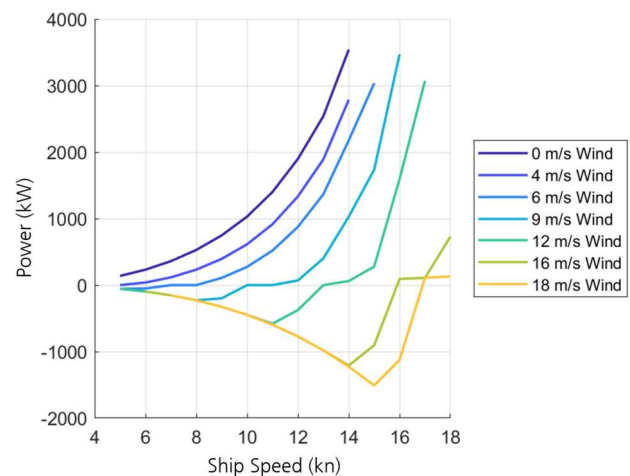
**Figure 4.** Characteristic curves of the propeller and the turbine. (This figure is available in colour online.)

which in combination with the maximum available wind propulsion is required to achieve the ship speed. Negative power represents the mechanical breaking power as a sum on both turbine shafts to hold the ship speed in combination with the wind propulsor. With increasing ship speed the recuperation power increases, however less than the inverse propulsion power. This is because the maximum power output of the turbine is linked to the ship speed or turbine inflow speed and limited by the maximum torque on the turbine shaft. While at a wind speed of 9 m/s a maximum recuperation potential of approx. 50 kW is calculated, a wind speed of 18 m/s enables a recuperation capacity of up to 1500 kW. High recuperation levels in the megawatt range require ship speeds higher than 14 kn and wind speeds of more than 15 m/s. The curves at 6–12 m/s wind show a range for which the calculated power is zero. Although resistance is generated by the turbine in this case, the flow is too low to enable recuperation.

3.2. Route simulation and speed optimization

The ship response matrix was fed into the route simulation. For a selected range of start dates the hourly wind and wave conditions were taken from the ERA5 reanalysis dataset (Copernicus Climate Change Service (C3S) 2020; Hersbach et al. 2020). On a direct route the weather data was assigned operating on a constant speed or a varying speed, in the case of speed optimization.

Speed optimization was carried out to maximize the ship's use of wind energy over a given voyage, by increasing travel in favourable weather conditions enabled by direct wind propulsion, minimizing the

**Figure 5.** Power profiles from the ship response matrix. Can we get more smoothed version of this? (This figure is available in colour online.)

required deployment of onboard energy, and avoiding unfavourable weather conditions.

The cost function to be minimized was defined as the net energy consumed by the ship over the voyage, calculated as the time integral of the rate of energy change of the energy system \dot{E} . The cost function can be represented mathematically by Equation (10a). The rate of energy change of the energy system can be correlated with the propulsion power and the recuperation power of the ship using the corresponding efficiencies η_{prop} and η_{recup} respectively, as shown in Equation (10b). The net power of the ship P_{ship} for any given ship speed v_{ship} under developing weather conditions obtained from ERA5, was obtained from the ship response matrix described in Sections 2 and 3.1. The net power of the ship was positive for propulsion and negative for recuperation. The cost function is therefore presented in discrete form as shown in Equation (10c). The 'state' for this dynamic system was defined to be the time delay $\tau_D[k]$ at any point with respect to the ship travelling at constant speed v_{ship}^{avg} , as shown in Equation (11).

$$J_{cost} = \int_0^T \dot{E}(t) dt = \int_0^D \frac{\dot{E}(t)}{v_{ship}(t)} dx \quad (10a)$$

$$\dot{E} = \begin{cases} P_{ship} \frac{1}{\eta_{prop}} & \text{if } P_{ship} > 0 \\ P_{ship} \eta_{recup} & \text{if } P_{ship} \leq 0 \end{cases} \quad (10b)$$

$$J_{cost} = \sum_{k=1}^N \left[\left(\frac{P_{ship}[k]}{\eta_{prop}} \right) (P_{ship}[k] > 0) \right] + \left[\eta_{recup} P_{ship}[k] (P_{ship}[k] < 0) \right] \left[\frac{d[k]}{v_{ship}[k]} \right] \quad (10c)$$

$$\tau_D[k] = \tau_D[k-1] + \frac{d[k]}{v_{ship}[k]} - \frac{d[k]}{v_{ship}^{avg}} \quad (11)$$

K is the maximum time delay at the end of the voyage, defined as the difference between the actual time at which the ship reaches the destination and the expected time at which it would have reached the destination if it had travelled at constant speed v_{ship}^{avg} .

The following assumptions and constraints were used in the optimization:

- The average ship speed during the entire voyage is at least 10 kn (and in another group of cases, at least 7 kn).
- The ship speed in each section is at least 5 kn and at most 15 kn.
- The ship is not operated when wind speeds exceed 17 m/s and wave heights exceed 5 m (corresponding to the Beaufort scale 8 and above).
- The discrete distance steps d_k are no more than 50 km and the ship is assumed to be travelling at a constant optimized speed within a step.
- The maximum delay (or advance) at each distance step is 15% of the total journey time.

For the model vessel and the two baseline cases we simulated 240 trips from Hamburg to New York and vice versa distributed over 10 years to capture seasonal as well as annual weather variation. This range of start dates and directions we applied for two average ship speeds of 10 and 7 kn. While 10 kn is at the lower spectrum of typical bulkier operation speeds, obtained from the ship technical data base, Clarksons World Fleet Register, 7 kn represents a significant lowering compared to regular operation. By lowering the ship speed we intended to increase the impact of the wind propulsor over the propeller and analyzed the difference in the impact of the hydrogenerator. On the other hand, this increased the voyage time from 14.1 days at 10 kn to 20.1 days at 7 kn. Furthermore, the simulations were distinguished between constant speed and optimized speed operation. The speed optimization algorithm allowing for enhancing the use of wind fields was utilized for the intermediate baseline and model vessel, which are equipped with sails. For the conventional baseline it was not applied since the effect is minimal. The conventional baseline is more sensitive to wave fields, which are more consistent over time and difficult to avoid by adjusting the vessel's speed only.

Figure 6 shows a sample crossing of the model ship between Hamburg and New York passing through varying wind fields, which are obtained from the ERA5

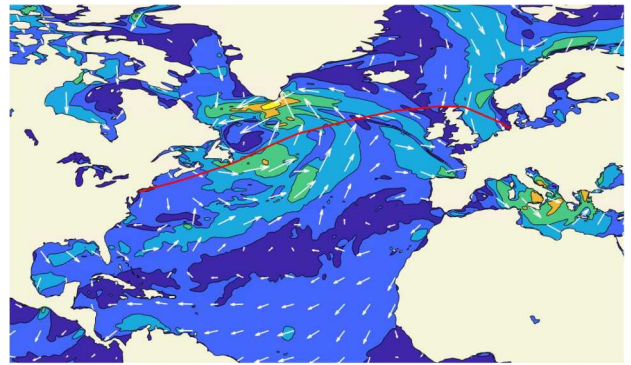


Figure 6. Route simulation between Hamburg and New York under varying wind conditions. (This figure is available in colour online.)

reanalysis data set. The speed within each sequence of a maximum length of 50 km and timing of the submer-sion of the recuperation turbines is controlled by the speed optimization.

3.3. Energy system model

The ship energy system was modelled in MATLAB Simulink. While profiles for propulsion power and recuperated power were obtained from the route simu-lation, the auxiliary load was assumed to be constant according to the ship type and size. Reference values were obtained from International Maritime Organiz-ation (2020)

The energy system models were built for the different powertrain configurations of the baseline, intermediate baseline and model ship to obtain results on energy efficiency and fuel consumption.

The baseline ship was modelled with a two-stroke HFO engine with a purely mechanical powertrain. For the mechanical powertrain the SFOC curves of the MAN 6S80ME-C8.2 engine were used, and a gearbox efficiency of 95% was assumed. The auxiliary power was provided by a separate auxiliary genset.

The intermediate baseline was equipped with the large Dynarig and an electrified powertrain similar to the model ship, but not using a hydrogenerator and a battery. The intermediate baseline was calcu-lated with two engine types, a HFO two-stroke and a methanol two-stroke engine. The efficiency is assumed to be the same for the methanol engine, but a fuel energy conversion based on the lower heat-ing values of the fuels is performed to calculate the fuel consumption.

The energy system of the model ship was required to switch between two modes during each crossing: recu-peration and energy provision, indicated by the positive and negative power values from the RMS. Figure 7 shows the energy system model structure with a reduced scope of participants operating on a DC power system. In recuperation mode the hydrogenerators produce

power which is rectified and fed to the main switch gear. The generated power is primarily used to feed the auxiliary power demands of the ship. If excess power is available, the power flow is split to additionally charge the battery system. In the energy provision mode the ship energy system needs to provide for the propul-sion and auxiliary power demands from its energy reserves. If the battery is charged, first the electric charge of the battery is utilized. This mitigates starting the methanol combustion engine for short periods. The bat-tery is discharged down to a state-of-charge, which leaves a power reserve for peak shaving. If the battery system is depleted the methanol genset is started.

3.4. Techno-economic model

The energy system was evaluated on the basis of the speed optimized power profiles derived in the route simulation module, considering different sizes of the energy system components. The aim was to calculate the size of the components needed to minimize the total cost (initial, operating, replacement and carbon costs) while accounting for weight and volume of these components. A design of experiments (DOE) was created by associating a range of values to each par-ameter, fixing the samples in each range, and generating a full factorial design using these samples. For each combination in the DOE, the energy system was simu-lated. The net fuel consumption, battery usage, and the considered sizes were then used to calculate the cost metrics, system weight and volume.

To identify the most favourable battery sizing match-ing the two hydrogenerators, the battery energy capacity was varied according to a brute force DOE repeating the energy system simulations and using the ranges shown in Table 4.

The economic metrics were then calculated based on the cost and density assumptions defined in Appen-dices 1 and 2. A cyclic battery lifetime for typical lithium ion cells was derived from datasheets but the maximum lifetime was limited to 15 years assuming that it accounts for the calendar life limitationsa as well (Korberg et al. 2021). The cost and densities of the methanol genset were derived from the cost and densities of the methanol engine and motor. Since the cost of marine turbines is typically unavailable in

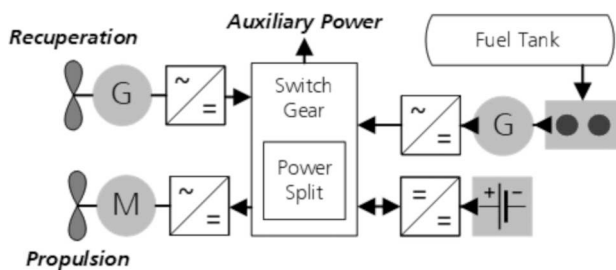


Figure 7. Ship energy system model. (This figure is available in colour online.)

Table 4. Example design of experiments.

Component	Lower Bound	Upper Bound	# of Samples
Battery (kWh)	1000	5000	5
Methanol Genset (kW), 7 kn	2500	3500	3
Methanol Genset (kW), 10 kn	3500	4500	3

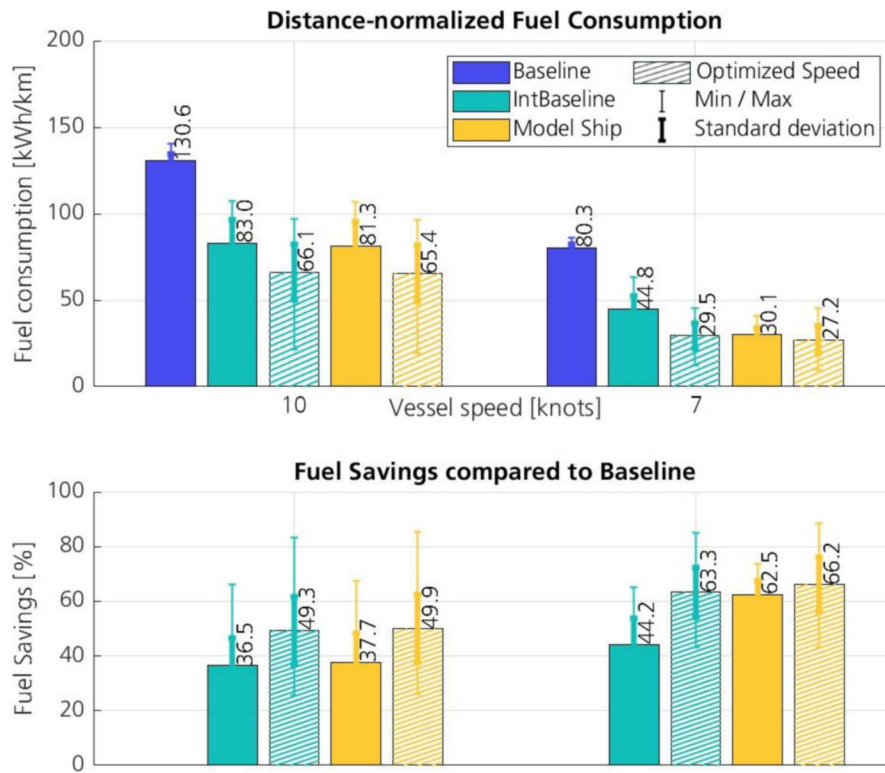


Figure 8. Distance normalized fuel consumption for the three analyzed power train options: Baseline without sails and a diesel combustion engine; Intermediate Baseline with sails and an electrified methanol engine power train; Model Ship, utilizing sails, a methanol engine and a hybridized power train with a battery and hydrogenerator. (This figure is available in colour online.)

open literature, it was assumed using expert knowledge available in the organization. The emission factor of green methanol was assumed to be 0. The baseline cargo carrying capacity was calculated based on estimations of light weight, weight of the hull structure, weight of the cargo tank and other onboard machinery. The bulk freight cost was assumed to exclude any fuel costs for this study.

3.5. Results

Figure 8 presents a comparison of the energy efficiency between the baseline cases and the model ship with the largest considered battery system of 3100 kWh, allowing for the highest impact of recuperation on the vessel energy use. The distance normalized fuel consumption is averaged over all trips, of each powertrain option. Since the cases operate on different fuels (Diesel and Methanol) the respective consumed fuel amounts are converted to the energy content of the fuel to analyze the energy efficiency of each powertrain upgrade. The conventional baseline (blue) requires on average 130.6 kWh/km at 10 kn and 83.0 kWh/km at 7 kn and operating on a constant speed. The implementation of the large sails for the intermediate baseline (green) leads

to a strong reduction in energy use down to 83.0 kWh/km and 44.8 kWh/km for the two speeds respectively. This equals energy savings of 36.5% and 44.2% compared to the baseline case. It can be observed that the implementation of sails leads to a larger spread in the minimum and maximum values as well as the standard deviation, because of the higher sensitivity to the weather conditions compared to the baseline. As a third step the implementation of the speed-optimization on the intermediate baseline case can be seen in the hatched green bars. This further increases the energy savings to 49.3% at 10 kn and 63.3% at 7 kn. The model ship with sails and a recuperation system is depicted in the yellow bars. The effect of implementing the recuperation system has little effect on the 10 kn case with an improvement of 1.2% at constant and 0.6% at optimized speed compared to the intermediate baseline. On the 7 kn case this effect is a little enhanced since the hydrogenerator is used more frequently. Here the model ship achieves for constant speed 18.3% and for optimized speed 3.1% more fuel savings than the intermediate baseline case. Overall it was found that the speed-optimization algorithm has a much larger benefit on energy efficiency of a sailing ship than the implementation of the hydrogenerator. For the hydrogenerators

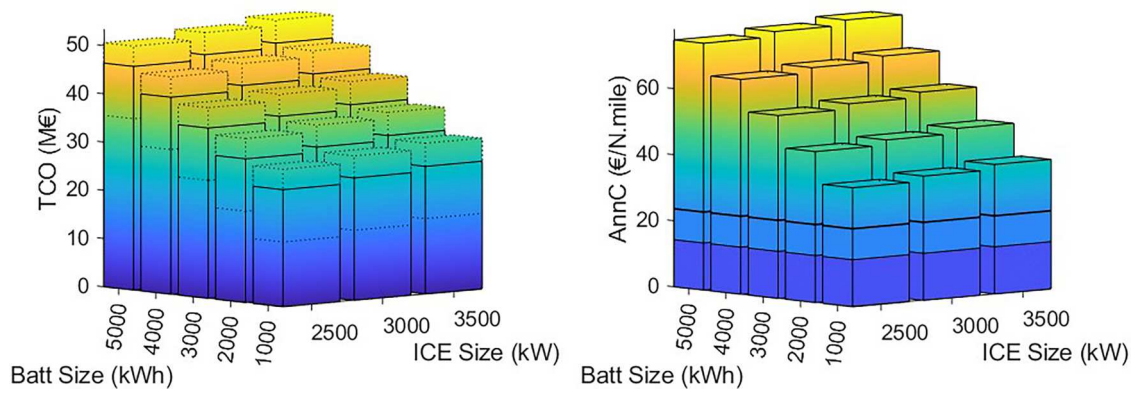


Figure 9. Impact of energy system size on total cost of ownership (left) and annualized cost (right) at 7 kn. The dotted lines on the left figure indicate the variation in TCO due to wind conditions. The figure on the right compares the annualized cost of the model ship to the baseline without sails (line above dark blue) and the intermediate baseline with Sails but without recuperation (thick line above medium blue). (This figure is available in colour online.)

an improved adaption to the weather conditions experienced most frequently might enhance its impact.

Figure 9 shows the variation in TCO and annualized cost with the considered genset and battery sizes at 7 kn. As the battery and genset size increases, the TCO increases as well, implying that the fuel consumption benefit obtained at higher battery sizes is not enough to compensate for the increased system cost. A similar trend is seen in the annualized cost as well. The annualized cost increases from 14 EUR/N.mile for the baseline (line

above dark blue) without sails to 36 EUR/N.mile for the Model ship, with the smallest battery and genset size, and increases further with the battery and genset sizes. The intermediate baseline versions with HFO and Methanol fuel achieve similar annualized cost of 24 EUR/N.mile (thick line above medium blue). The similarity in cost is because the higher cost of methanol is similar to the considered emissions cost of HFO, as will be seen later.

The top subplot in Figure 10 compares the TCO of all the considered powertrain variations at 7 kn. The hybrid

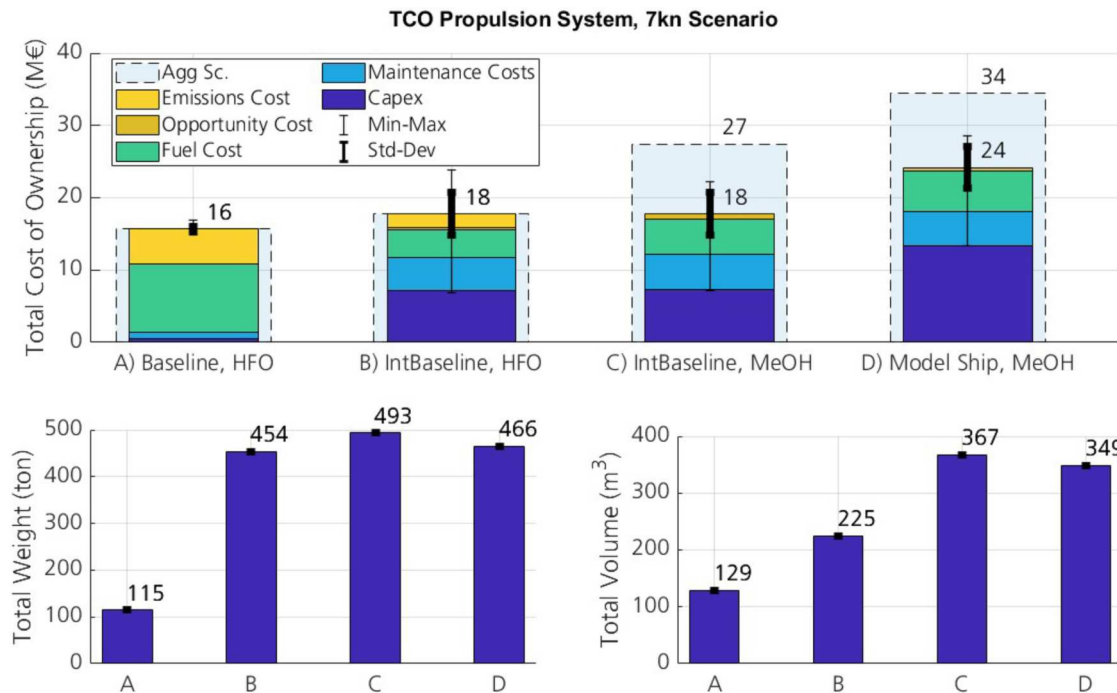


Figure 10. Comparison of the total cost of ownership (top), powertrain weight (bottom left) and volume (bottom right) between the considered powertrain options, at 7kn. The minimum TCO powertrain size was considered for the Model Ship option. The top figure additionally presents the contribution of initial, maintenance, fuel, emissions and opportunity costs, and the impact of aggressive cost scenario. The error bars indicate the effect of wind conditions. (This figure is available in colour online.)

powertrain size with minimum TCO is chosen here for the Model Ship. The thin error bars indicate the min-max variation in TCO due to wind, and the thick error bars indicate the standard deviation. The TCO of the HFO based powertrain without sails is the least, while the additional costs of the masts and sails increase the TCO of the powertrains with sails. The fuel consumption reduction is not sufficient to offset the extra cost of the masts and sails. But with increasing carbon costs and potentially reducing the cost of sails with maturity, the options with wind assisted propulsion could become more favourable.

The TCO of the powertrains of the intermediate baselines with HFO (B) and Methanol (C) are equal in the conservative scenario, as the extra costs of the methanol engine, tank and fuel offset the emissions cost of HFO. The intermediate baselines have just slightly higher TCO than the baseline scenario, because the introduction of sails effectively reduces the fuel consumption and emission costs.

For the recuperating powertrain of the Model Ship (D), the average TCO increases by 33% over the intermediate baseline with methanol (C) in the conservative scenario, which would reduce as the costs for the hybrid components drop with improving technology readiness levels. Under the aggressive cost scenario of methanol, the TCO of D are 26% higher than C. While the hybrid system results in higher TCO it is providing the flexibility for recuperating energy under excess wind and potential for better performance in the future with implementing wind routing also.

The bottom subplots compare the weight and volume across the considered options. The introduction of sails introduces extra weight into the system, which reduces the cargo capacity of the ship (A compared to B-D). From an economic perspective this is reflected in the opportunity cost as shown in the upper TCO plot, however the impact is small.

4. Discussion and summary

In this paper, we presented the Odyssa framework that allows for the holistic evaluation of windship designs. We combined various modelling approaches that include the ship hydro- and aerodynamics, route simulation in relevant operating conditions, operation optimization of the voyage speed, energy system simulation as well as the evaluation of technical and economic parameters. Odyssa is designed as a modular toolbox that allows for a fast adaptation to specific windship designs. In the second part we utilized Odyssa to investigate a wind ship design of a 130 m cargo ship equipped with a Dynarigg, a

recuperation turbine and a methanol engine operating on a transatlantic route from Hamburg to New York. The different models utilized to simulate this case were presented.

For the vessel performance we implemented an aero- and hydrodynamic model, based on a 4-DOF model including sails, hull, appendages, propeller and turbine. We utilized empirical formulas to model the ship hull, appendages, and sail system in the case study of a fictional ship application. Upon validation of the hull forces with CFD, a strong correlation was observed with calm water resistance, showing a deviation of only 3% up to 15 kn and increasing to a maximum overestimation of 8% at 17 kn. However, in drifting conditions an overestimation of up to 20% was observed, particularly at higher speeds. This leads to a tendency of more conservative results. For an actual ship design, the direct incorporation of data from CFD or measurement campaigns of a combined hull and sail model would enhance the model fidelity and predictive accuracy. Odyssa allows for the integration of CFD as well as model test data.

In the route simulator we applied varying wind and wave conditions of the ERA5 dataset along the trip, which allows to represent developing weather along each trip instead of statistical averaged data. Yet, the use of steady-state modelling in hourly time steps does not capture the dynamic behaviour of a windship system and simplifies transient behaviour such as wind fluctuation, dynamic ship movement and resulting transient loads, particularly the fluctuations in engine load caused by wind gusts during hybrid operations involving wind propulsion. We expect a mild underestimation of required propulsive power from this effect.

The speed of the ship is optimized with a dynamic programming approach to minimize the energy consumption on the trip based on the ERA5 hindsight data. In practical applications, reliance on forecast data would be necessary, but this introduces significant uncertainty, especially when predicting conditions multiple days in advance. A real world application would therefore require to address these uncertainties in the algorithm. Moreover, ERA5 data is averaged over large areas, and may not accurately represent localized weather conditions. This discrepancy is particularly significant in coastal areas, where the wind boundary layer and wave fields exhibit greater variability. Since the speed optimization algorithm is sensitive to this variability, we expect a mild overestimation of the energy savings compared to a real world application.

Furthermore the energy system is modelled based on efficiency data of various components to investigate

the ships fuel consumption. While we include machinery limitations such as maximum loading conditions, transient effects between states are neglected similar to the vessel performance model. This might lead to a slight underestimation of the fuel consumption. At an operating speed of 10 kn our results show a reduction of 36.5% in fuel consumption by the incorporation of the large Dynarig System. These savings can be further enhanced to 49.3% by applying the speed optimization algorithm and increasing the utilization of favourable wind conditions. The incorporation of the hydroturbine is effective only at a smaller operating speed of 7 kn, where an additional improvement of 3.1% can be achieved.

We applied a DOE for the model ship to investigate the most favourable powertrain rating and battery size matching the recuperation potential. In our future work, we intend to expand this design exploration also to the hull and sail system and incorporate further technologies such as various sail types. The economic metrics derived from our analysis are contingent on cost assumptions, which can differ widely for emerging technologies, such as wind propulsors and methanol engines, as well as for various renewable fuels used in shipping. We took into account an aggressive scenario for higher costs of methanol components and fuel price as a means of a sensitivity study. However, a detailed sensitivity analysis of carbon tax is out of scope of the paper. The variations in cost assumptions can significantly influence the overall economic viability of the technologies being studied. This uncertainty can be mitigated the more developed a design project is and specific equipment is selected. Based on the cost assumptions in this study the smallest battery capacity of one MWh was found as the most economic solution since the recuperation energy is low. We investigated the TCO of the different ship designs considering the usage of different fuels, heavy fuel oil and methanol. The windship designs achieve a reduction of 48–55% in fuel costs and have 1–3% lower operating costs than a conventional ship despite increased maintenance costs on the sail system. Yet their overall costs of ownership are majorly influenced by the high additional investment costs of the large sail system. The intermediate baseline designs with sails and without a recuperation system are close to compete with the conventional baseline case over their life cycle. For the model ship with a recuperating system we found 33% higher TCO, due to higher investment costs and insufficient fuel savings to compensate those. Further development and effects of economy of scale would be necessary to create a positive business case for the investigated ship design and operational parameters.

Disclosure statement

No potential conflict of interest was reported by the author(s).

ORCID

Annika Fitz  <http://orcid.org/0000-0002-6064-0451>

Dheeraj Gosala  <http://orcid.org/0000-0002-4098-1603>

Vaidehi Gosala  <http://orcid.org/0000-0001-9709-8371>

Tobias Lampe  <http://orcid.org/0000-0002-8947-7379>

Thorben Schwedt  <http://orcid.org/0000-0002-2127-0494>

Sophie Stutz  <http://orcid.org/0009-0000-3313-4468>

Sören Ehlers  <http://orcid.org/0000-0001-5698-9354>

Data availability statement

The authors confirm that the data supporting the findings of this study are available within the article and its supplementary materials.

References

- Aider CA. 2023. Integration of a tank storage solution for alternative fuels on a ro-ro ship. In: *Advances in the analysis and design of marine structures*. London: CRC Press. p. 761–771. doi: [10.1201/9781003399759-84](https://doi.org/10.1201/9781003399759-84).
- Alfonsin V, Suarez A, Urrejola S, Miguez J, Sanchez A. 2015. Integration of several renewable energies for internal combustion engine substitution in a commercial sailboat. *Int J Hydrogen Energy*. 40(20):6689–6701. doi: [10.1016/j.ijhydene.2015.02.113](https://doi.org/10.1016/j.ijhydene.2015.02.113).
- Allwright G. 2024 Feb 15. Opinion: can wind propulsion weather the approaching perfect storm? *Offshore Energy*. [accessed: 2025 May 7th]; Propulsion. <https://www.offshore-energy.biz/opinion-can-wind-propulsion-weather-the-approaching-perfect-storm/>.
- Babarit A, Clodic G, Delvoye S, Gilloteaux JC. 2020. Exploitation of the far-offshore wind energy resource by fleets of energy ships. part a. energy ship design and performance. *Wind Energy Sci*. 5(3):839–853. doi: [10.5194/wes-2019-100](https://doi.org/10.5194/wes-2019-100).
- Barnitsas MM. 1981. KT, KQ and efficiency curves for the wageningen B-series propellers. Ann Arbor (MI), USA: University of Michigan. p. 1–6.
- Bertram V. 2011. *Practical ship hydrodynamics*. 2nd ed. Burlington: Elsevier Science. p. 285–298.
- Blendermann W. 1994. Parameter identification of wind loads on ships. *J Wind Eng Ind Aerodyn*. 51(3):339–351. doi: [10.1016/0167-6105\(94\)90067-1](https://doi.org/10.1016/0167-6105(94)90067-1).
- Bordogna G, Keuning JA, Huijsmans R, Belloli M. 2018. Wind-tunnel experiments on the aerodynamic interaction between two rigid sails used for wind-assisted propulsion. *Int Shipbuild Prog*. 65(1):93–125. doi: [10.3233/ISP-180143](https://doi.org/10.3233/ISP-180143).
- Bronstein IN, Semendjajew KA. 1977. *Taschenbuch der Mathematik für Ingenieure und Studenten der technischen Hochschulen*. 17th ed. Leipzig: BSB B.G. Teubner Verlagsgesellschaft. p. 117.
- Bui KQ, Perera LP, Emblemavåg J. 2022. Life-cycle cost analysis of an innovative marine dual-fuel engine under

- uncertainties. *J Clean Prod.* 380(2):134847. doi: [10.1016/j.jclepro.2022.134847](https://doi.org/10.1016/j.jclepro.2022.134847).
- Cole W. 2021. Cost projections for utility-scale battery storage: 2021 update. Golden (CO). doi: [10.2172/1786976](https://doi.org/10.2172/1786976).
- Copernicus Climate Change Service (C3S). 2020. Era5 hourly data on single levels from 1940 to present. Climate Data Store (CDS). doi: [10.24381/CDS.ADBB2D47](https://doi.org/10.24381/CDS.ADBB2D47).
- de Vries N. 2019. Safe and effective application of ammonia as a marine fuel [master's thesis]. Delft: Delft University of Technology and C-JOB. p. 54.
- Dykstra Naval Architects. 2013. The ecoliner concept: future design in progress. Amsterdam: Dykstra Naval Architects.
- Ekinci S, Alvar M. 2017. Horizontal axis marine current turbine design for wind-electric hybrid sailing. *Brodogradnja.* 68(2):127–151. doi: [10.21278/brod68209](https://doi.org/10.21278/brod68209).
- European Commission. 2023. Electricity prices for non-household consumers. Eurostat. [accessed: 2025 Mar 21st]. https://ec.europa.eu/eurostat/statistics-explained/index.php?title=Electricity_price_statisticsElectricity_prices_for_non-household_consumers.
- Ghassemi M. 2020. High power density technologies for large generators and motors for marine applications with focus on electrical insulation challenges. *High Voltage.* 5(1):7–14. doi: [10.1049/hve.2019.0055](https://doi.org/10.1049/hve.2019.0055).
- Goh K. 2017. Wind powered ships with hybrid autonomous technologies. In: Royal Institution of Naval Architects, editor. *Proceedings of the International Conference on Power and Propulsion Alternatives for Ships 2017*. London: Curran Associates Inc.. p. 29–38.
- Hersbach H, Bell B, Berrisford P, Hirahara S, Horányi A, Muñoz-Sabater J, Nicolas J, Peubey C, Radu R, Schepers D, et al. 2020. The era5 global reanalysis. *Q J R Meteorol Soc.* 146(730):1999–2049. doi: [10.1002/qj.3803](https://doi.org/10.1002/qj.3803).
- Holtrop J, Mennen G. 1982. An approximate power prediction method. *Int Shipbuild Prog.* 29(335):166–170. doi: [10.3233/ISP-1982-2933501](https://doi.org/10.3233/ISP-1982-2933501).
- Horvath S, Fasihi M, Breyer C. 2018. Techno-economic analysis of a decarbonized shipping sector: technology suggestions for a fleet in 2030 and 2040. *Energy Convers Manag.* 164(1):230–241. doi: [10.1016/j.enconman.2018.02.098](https://doi.org/10.1016/j.enconman.2018.02.098).
- International Maritime Organization. 2020. Reduction of greenhouse gas emissions from ships: fourth IMO GHG study 2020. 53(9), pp. 1689–1699.
- International Renewable Energy Agency. 2021. Innovation outlook renewable methanol. Abu Dhabi: IRENA. [accessed: 2025 May 7th]. https://www.irena.org/-/media/Files/IRENA/Agency/Publication/2021/Jan/IRENA_Innovation_Renewable_Methanol_2021.pdf. p. 85.
- Istrate IR, Iribarren D, Dufour J, Ortiz Cebolla R, Arrigoni A, Moretto P, Dolci F. 2022. Quantifying emissions in the european maritime sector. Luxembourg: Publications Office of the European Union. doi: [10.2760/496363](https://doi.org/10.2760/496363).
- Juliá E, Tillig F, Ringsberg JW. 2020. Concept design and performance evaluation of a fossil-free operated cargo ship with unlimited range. *Sustainability.* 12(16):6609. doi: [10.3390/su12166609](https://doi.org/10.3390/su12166609).
- Korberg AD, Brynolf S, Grahn M, Skov IR. 2021. Techno-economic assessment of advanced fuels and propulsion systems in future fossil-free ships. *Renew Sustain Energy Rev.* 142:110861. doi: [10.1016/j.rser.2021.110861](https://doi.org/10.1016/j.rser.2021.110861).
- Kramer JV, Steen S. 2022. Sail-induced resistance on a wind-powered cargo ship. *Ocean Eng.* 261:111688. doi: [10.1016/j.oceaneng.2022.111688](https://doi.org/10.1016/j.oceaneng.2022.111688).
- Liu P, Bose N, Chen K, Xu Y. 2018. Development and optimization of dual-mode propellers for renewable energy. *Renew Energy.* 119(1):566–576. doi: [10.1016/j.renene.2017.12.041](https://doi.org/10.1016/j.renene.2017.12.041).
- Lloyds Register, UMAS. 2020. Techno-economic assessment of zero-carbon fuels. [accessed: 2025 May 7th]. <https://www.lr.org/en/knowledge/research-reports/2020/techno-economic-assessment-of-zero-carbon-fuels/>.
- Mason J, Larkin A, Gallego-Schmid A. 2023. Mitigating stochastic uncertainty from weather routing for ships with wind propulsion. *Ocean Eng.* 281:114674. doi: [10.1016/j.oceaneng.2023.114674](https://doi.org/10.1016/j.oceaneng.2023.114674).
- Mobron E. 2014. Improving the performance of a sail-assisted cargo vessel [Doctoral thesis]. Delft University of Technology.
- Molland AF, Turnock SR, Hudson DA. 2011. Ship resistance and propulsion: practical estimation of ship propulsive power. Vol. 1. Cambridge (UK): Cambridge University Press. p. 60.
- NEOLINE. 2023. Neoline turns its neoliner pilot project into a reality and launches the construction of its first 136m sailing cargo ship. [accessed: 2025 May 7th]. <https://www.neoline.eu/en/neoliner-under-construction/>.
- Ouchi K, Shima K, Kimura K. 2023. 'wind hunter' -- the zero emission cargo ship powered by wind and hydrogen energy. In: Royal Institution of Naval Architects, editor. *Proceedings of the Wind Propulsion Conference 2023*. London: Curran Associates Inc. p. 81–88.
- Perez S, Guan C, Mesaros A. 2021. Economic viability of bulk cargo sailing ships. *Journal of Merchant Ship Wind Energy.* [accessed: 2025 May 7th]. https://www.jmwe.org/uploads/1/0/6/4/106473271/jmwe_17_august_2021.pdf.
- PowerTech Systems. 2025. Lithium iron phosphate battery. [accessed: 2025 Mar 21st]. <https://www.powertechsystems.eu/home/tech-corner/lithium-iron-phosphate-lifepo4/>.
- Reche-Vilanova M, Hansen H, Bingham HB. 2021. Performance prediction program for wind-assisted cargo ships. *J Sailing Technol.* 6(1):91–117. doi: [10.5957/jst/2021.6.1.91](https://doi.org/10.5957/jst/2021.6.1.91).
- Sandia National Laboratories (SNL). 2020. Feasibility study of replacing the R/V robert gordon sproul with a hybrid vessel employing zero-emission propulsion technology: a comparison of hydrogen fuel cell and battery hybrid technologies for a coastal/local research vessel application. Livermore (CA): SNL. p. 32.
- Seguin V, Arnaud E, Zanuttini J, Pean G, Dupuy M, Mousselon O. 2019. Neoliner 136 m, a veliced cargo vessel, allowing a major reduction in consumption fossil energy and associated emissions. *Bulletin de l'Association Technique Maritime et Aéronautique.*
- Ship and Bunker. 2024. Rotterdam bunker prices -- ship & bunker (shipandbunker.com). [accessed: 2024 May 24th]. <https://shipandbunker.com/prices/emea/nwe/nl-rtm-rotterdam#VLSFO>.
- Singleton T. 2023 Aug 21st. Pioneering wind-powered cargo ship sets sail. BBC News. [accessed: 2025 May 7th]. <https://www.bbc.com/news/technology-66543643>.
- Stolz B, Held M, Georges G, Boulouchos K. 2022. Techno-economic analysis of renewable fuels for ships carrying

- bulk cargo in europe. *Nat Energy*. 7(2):203–212. doi: [10.1038/s41560-021-00957-9](https://doi.org/10.1038/s41560-021-00957-9).
- Sun W, Tang S, Liu X, Zhou S, Wei J. 2022. An improved ship weather routing framework for cii reduction accounting for wind-assisted rotors. *J Mar Sci Eng*. 10(12):1979. doi: [10.3390/jmse10121979](https://doi.org/10.3390/jmse10121979).
- Taljegard M, Brynolf S, Grahn M, Andersson K, Johnson H. 2014. Cost-effective choices of marine fuels in a carbon-constrained world: results from a global energy model. *Environ. Sci. Technol.* 48(21):12986–12993. doi: [10.1021/es5018575](https://doi.org/10.1021/es5018575).
- Talluri L, Nalianda DK, Giuliani E. 2018. Techno economic and environmental assessment of flettner rotors for marine propulsion. *Ocean Eng*. 154:1–15. doi: [10.1016/j.oceaneng.2018.02.020](https://doi.org/10.1016/j.oceaneng.2018.02.020).
- Talluri L, Nalianda DK, Kyprianidis KG, Nikolaidis T, Pilidis P. 2016. Techno economic and environmental assessment of wind assisted marine propulsion systems. *Ocean Eng*. 121:301–311. doi: [10.1016/j.oceaneng.2016.05.047](https://doi.org/10.1016/j.oceaneng.2016.05.047).
- Thies F, Ringsberg JW. 2022. Wind-assisted, electric, and pure wind propulsion – the path towards zero-emission roro ships. *Ships and offshore Structures*. 18(8):1–8. doi: [10.1080/17445302.2022.2111923](https://doi.org/10.1080/17445302.2022.2111923).
- Tillig F, Ringsberg JW. 2019. A 4 DOF simulation model developed for fuel consumption prediction of ships at sea. *Ships offshore Struct*. 14(sup1):112–120. doi: [10.1080/17445302.2018.1559912](https://doi.org/10.1080/17445302.2018.1559912).
- Tillig F, Ringsberg JW. 2020. Design, operation and analysis of wind-assisted cargo ships. *Ocean Eng*. 211:107603. doi: [10.1016/j.oceaneng.2020.107603](https://doi.org/10.1016/j.oceaneng.2020.107603).
- Tillig F, Ringsberg JW, Mao W, Ramne B. 2017. A generic energy systems model for efficient ship design and operation. *J Eng Marit Environ*. 231(2):649–666. doi: [10.1177/1475090216680672](https://doi.org/10.1177/1475090216680672).
- van der Kolk N, Bordogna G, Mason JC, Despraïries P, Vrijdag A. 2019. Case study: wind-assisted ship propulsion performance prediction, routing, and economic modelling. In: Royal Institution of Naval Architects, editor. *Proceedings of the International Conference Power & Propulsion Alternatives for Ships 2019*. London: Curran Associates Inc.
- van der Meulen S, Grijspaardt T, Mars W, Van der Geest W, Roest-Crollius A, Kiel J. 2020. Cost figures for freight transport—final report. Zoetermeer: Panteia.
- van der Plas MD, Hillege L, de Vos P. 2024. The impact of hydro generation on board large sailing yachts. In: *Proceedings of 15th International Marine Design Conference (IMDC-2024)*. TU Delft OPEN Publishing. doi: [10.59490/imdc.2024.906](https://doi.org/10.59490/imdc.2024.906).
- Victron Energy. 2023. Datasheet of 12,8 & 25,6 volt lithium-iron-phosphate batteries smart. Almere: Victron Energy.
- watt&sea. 2025. Cruising 600 hydrogenerator. [accessed: 2025 May 7th]. <https://www.wattandsea.com/en/hydrogenerators/cruising-600-en/>.

Appendices

Appendix 1. Cost assumptions

Component	Source	per mass	per volume
Battery	Stolz et al. (2022)	0,4 kWh/kg	470 kWh/m ³
Diesel Engine	de Vries (2019)	0,035 kW/kg	32 kW/m ³
Methanol Genset	Expert Assumption	0.03 kW/kg	28.37 kW/m ³
Motor	Ghassemi (2020)	0,43 kW/kg	250 kW/m ³
Rig	Mobron (2014)	63 ton/mast	--
Diesel tank	Aider (2023)	8 kWh/kg	7000 kWh/m ³
Methanol tank	Aider (2023)	5,4 kWh/kg	2790 kWh/m ³

Appendix 2. Power and energy density assumptions

Component	Source	Unit	Cons.	Agg.
Variable Assumptions				
Li-ion Battery	Sandia National Laboratories (SNL)	EUR/kWh	500	600
Battery Lifetime	PowerTech Systems (2025), Victron Energy (2023), (max 15 years Korberg et al. 2021)	cycles	2000	1500
Methanol Genset	Expert Assumption	EUR/kW	700	920
Methanol Engine	Korberg et al. (2021), Taljegard et al. (2014)	EUR/kW	500	720
Methanol	International Renewable Energy Agency (2021)	EUR/kg	0.4	1
Electricity	European Commission (2023)	EUR/kWh	0.1	0.3
Fixed Assumptions				
Diesel Engine	Korberg et al. (2021)	EUR/kW	460	
Power Electronics	de Vries (2019), Cole (2021)	EUR/kW	400	
Motor	de Vries (2019), Lloyds Register, UMAS (2020)	EUR/kW	200	
Turbines	Expert Assumption	EUR/turbine	50,000	
Diesel Tank	Korberg et al. (2021)	EUR/MWh	70	
Methanol Tank	Korberg et al. (2021)	EUR/MWh	120	
Rig	Goh (2017)	EUR/system	5,000,000	
Sails	Perez et al. (2021)	EUR/m ²	30	
Diesel Fuel	Ship (2024)	EUR/GJ	15.33	
Engine Maintenance	Bui et al. (2022)	%	5	
Emission Factor -- HFO	Istrate et al. (2022)	t CO ₂ /ton	3.114	
Carbon Cost	Bui et al. (2022)	EUR/ton	100	
Bulk Freight Cost	van der Meulen et al. (2020)	EUR/mt/mile	0.004	
Discount Rate	Taljegard et al. (2014)	%	7	
Annual Days of Operation	Lloyds Register, UMAS (2020)	days	230	
Ship Lifetime	Taljegard et al. (2014)	years	30	
Rig Lifetime	Mobron (2014)	years	30	
Sails Lifetime	Perez et al. (2021)	years	2	